

Metamorphic evolution of amphibole-bearing aluminous gneisses from the Eastern Namaqua Province, South Africa

HUW C. HUMPHREYS*

Precambrian Research Unit, Department of Geology, University of Cape Town, 7700 Rondebosch, South Africa

ABSTRACT

Amphibole-bearing aluminous rocks from the 1.3 Ga Copperton Formation of the Namaqua Province, South Africa, preserve reaction textures consistent with near isobaric cooling. Peak metamorphic assemblages equilibrated at 600–820 °C and 5–6.5 kbar and include orthopyroxene + garnet + cordierite in the granulite facies and garnet + gedrite + cordierite + staurolite, gedrite + hornblende + cordierite + garnet, and cordierite + staurolite + sillimanite + hornblende in the amphibolite facies. All rocks contain oligoclase and quartz, whereas biotite is present in the amphibolite facies. Cordierite and hornblende have partially or completely altered to staurolite-, chlorite-, and gedrite-bearing assemblages in rehydration reactions, whereas sillimanite-bearing rocks developed kyanite on cooling. Interpretation of these textures using a petrogenetic grid in FMASH suggests a cooling path that is isobaric at pressures above that of the Al_2SiO_5 triple point. The latest textures in the rocks reflect a regrowth of garnet over chlorite + quartz and gedrite + staurolite, indicative of a final period of reheating. This is consistent with the metamorphic evolution of pelites along the strike of the amphibole-bearing rocks that show regrowth of garnet and staurolite from retrograde chlorite + muscovite substrates. Aluminous gneisses of the Copperton Formation preserve prograde and retrograde examples of the uncommon assemblage staurolite + sillimanite + hornblende. The prograde assemblage occurs at the interface of a hornblende-bearing semipelitic schist and a K_2O -poor peraluminous gneiss; the retrograde assemblage occurs as grain-boundary minerals at the margins of altered cordierite and plagioclase grains.

INTRODUCTION

Recent studies of aluminous rocks containing amphiboles have revealed the wealth of pressure-temperature information available from a consideration of their textures and phase relationships (Spear, 1977, 1978; Robinson et al., 1982; Harley, 1985; Hudson and Harte, 1985; Spear and Rumble, 1986; Baker et al., 1987; Schumacher and Robinson, 1987; Visser and Senior, 1990). These include the placement of peak temperatures and pressures using calibrated petrogenetic grids in $\text{FeO-MgO-Al}_2\text{O}_3\text{-SiO}_2\text{-H}_2\text{O}$ (FMASH) or $\text{Na}_2\text{O-CaO-FeO-MgO-Al}_2\text{O}_3\text{-SiO}_2\text{-H}_2\text{O}$ (NCFMASH) and the construction of P - T paths from the successive appearance of stable or metastable assemblages within a sample or group of samples. The reaction textures and mineral compositions in aluminous gneisses and schists of the Copperton Formation in Cape Province, South Africa, provide an opportunity to construct a P - T path from such amphibole-bearing rocks.

The aluminous rocks at Copperton include those with amphibole and those without. The latter approximate to

pelitic compositions and are described in Cornell et al. (1992). Amphibole-bearing varieties are found in the Copperton Formation at a variety of metamorphic grades. They contain the unusual assemblage sillimanite + hornblende + staurolite (\pm cordierite) and the more common assemblages gedrite + garnet + cordierite + staurolite and garnet + cordierite + hornblende + gedrite.

GEOLOGIC SETTING

The Copperton Formation is a northwest-striking unit of banded and interlayered gneisses adjacent to the tectonic boundary between the Kheis Belt, with an age between 3.0 and 1.7 Ga (Cornell et al., 1986), and the gneisses of the Kakamas Terrane, with an age between 1.6 and 1.0 Ga (Theart, 1985; Barton and Burger, 1983). The Copperton Formation is dated by the single-zircon U-Pb method at 1.29 Ga (Cornell et al., 1990b) and is interpreted on tectonic and geochemical grounds as an island arc sequence formed at the onset of the Namaqua orogenic cycle (Geringer et al., 1986). The Copperton Formation was deformed and metamorphosed at 1.22–1.20 Ga and remetamorphosed at 1.10–1.08 Ga (Cornell et al., 1990a). The textures described in this paper date from these two periods of metamorphism.

* Present address: 61 Pendre Gardens, Brecon, Powys, Wales LD3 9EP, U.K.

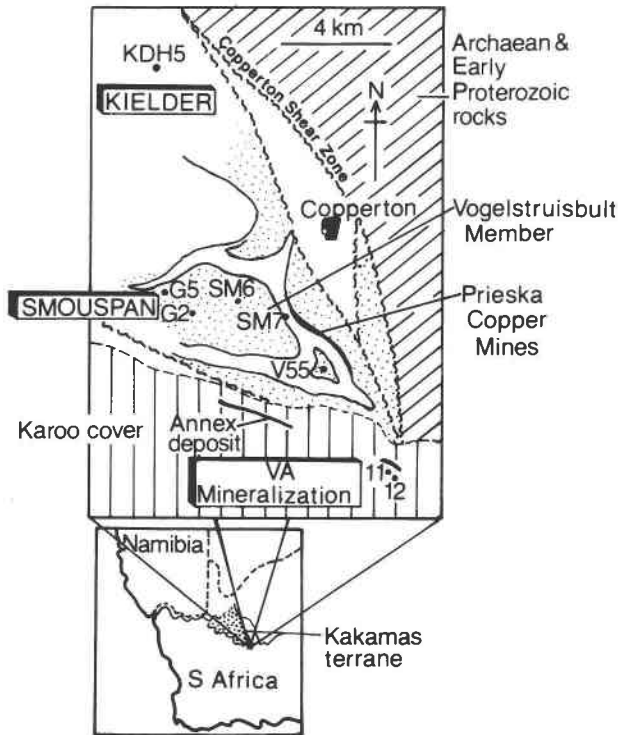


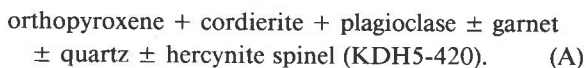
Fig. 1. Local geology of the Copperton region, from Humphreys et al. (1988b). Copperton is at the southeast corner of the Kakamas Terrane (inset).

LOCAL GEOLOGY AND PETROGRAPHIC DESCRIPTIONS

The samples described come from the wall rocks of three zones of pyritic mineralization near the Prieska Zn-Cu mine. All the samples were collected from within 15 km of one another (Fig. 1) and are found on the farms Kielder (three samples) and Smouspan (seven samples) and near the VA Cu-Fe deposit (three samples). Peak metamorphic conditions lie in the granulite facies at Kielder and in the eastern part of Smouspan and in the mid-upper amphibolite facies for the remainder. Mineral assemblages are in Table 1.

Kielder deposit

The Kielder Zn-Pb mineralization is hosted by magnesian, mafic, and intermediate granulites (Gorton, 1982). Temperatures are estimated at 750–850 °C by the garnet-orthopyroxene thermometer of Harley (1984), and pressures of 5.5–6.7 kbar are estimated from the garnet-orthopyroxene-plagioclase-quartz barometer of Powell and Holland (1988). The peak metamorphic assemblage in magnesian granulites is



Dehydration melting at the peak of metamorphism resulted in crosscutting pods of plagioclase + potassium

feldspar + orthopyroxene + cordierite that disrupted a pseudomorphed biotite schistosity. Both granulite-facies metamorphism and accompanying melting occurred after penetrative deformation.

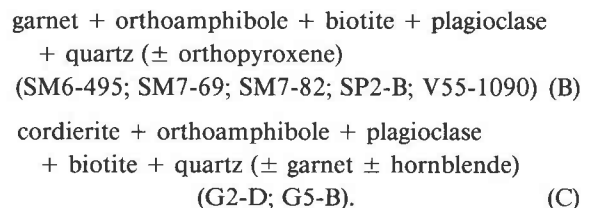
The three orthoamphibole-bearing specimens (KDH5-95, KDH5-105, and KDH5-420) are partially or fully retrograded granulites with heterogeneous distribution of minerals. KDH5-95 and KDH5-105 have large sheaves of clove gray anthophyllite with gedrite or hornblende margins, coarse intergrowths of cordierite and quartz, and coarse patches of plagioclase. Important retrograde textures in these two rocks include (1) the replacement of cordierite grain boundaries by staurolite + chlorite \pm gedrite (Fig. 2E), (2) the occurrence, at cordierite grain boundaries, of the assemblage sillimanite + gedrite as small euhedral grains (Fig. 2A), and (3) the coexistence of hornblende + staurolite + sillimanite as a grain boundary assemblage between plagioclase and cordierite. In 1, the product grains are euhedral and postdate what remains of the structural fabric of the original granulite. Chlorite overgrows staurolite and is the final mineral to form in the retrograde assemblage.

Decomposition of biotite and cordierite to the assemblage muscovite + kyanite + staurolite + chlorite is seen in the amphibole-free gneiss KDH5-544 and offers corollary evidence that the *P-T* path just after the peak of metamorphism near Copperton passed across the sillimanite-kyanite curve.

In KDH5-420, orthoamphibole has grown from Assemblage A along a band 2 mm wide, according to the reaction $\text{garnet} + \text{cordierite} + \text{orthopyroxene} + \text{potassium feldspar} + \text{H}_2\text{O} = \text{biotite} + \text{anthophyllite} + \text{quartz}$, representing the earliest retrogression of granulite facies assemblages at Kielder. Subsequent growth of secondary garnet grows across retrograde biotite and anthophyllite (Fig. 3a).

Smouspan biotite gneisses

Biotite + orthoamphibole-bearing gneisses with garnet occur in the Vogelstruisbult Member of the Copperton Formation on the farm Smouspan. The Vogelstruisbult Member is a banded sequence of amphibolite, calc-silicate gneiss, biotite-hornblende gneiss, and pelite that forms the stratigraphic hanging wall to the Prieska mine ore body. Five biotite-rich and two cordierite-rich gneisses were sampled by bore holes SM6, SM7, SP2, V55, G2, and G5. Two parageneses can be identified:



Assemblage B was derived from a granulite-facies precursor, and in some cases, orthopyroxene is still extant as heavily corroded and altered porphyroblasts. The pre-

TABLE 1. Mineral assemblages

Sample	Qtz	Pl	Grt	Crd	Oam	St	Sil	Ky	Bt	Opx	Hbl	Chl	Opaque
Kielder													
KDH5-95	—	x	—	x	x	—	—	—	x	—	—	—	Mag
KDH5-105	x	x	—	x	x	x	x	—	x	ps	x	x	Py
KDH5-420	x	x	x'	x	x	—	—	?	x	x	—	—	Mag
Smouspan													
V55-1090	13	25	6	—	24	—	—	—	31	—	—	—	Mag
SM6-495	1	25	2	—	8	—	—	—	49	12	—	—	Mag
SM7-69	x	x	x	—	x	—	—	—	x	—	—	—	Mag
SM7-82	—	47	3	—	8	—	—	—	30	12	—	—	Mag
SP2-B	x	x	x	—	x	—	—	—	x	ps	—	—	Mag
G2-D	39	33	—	3	4	2	3	?	15	—	—	2	Py
G5-B	35	13	10	ps	10'	14	?	?	15	—	2	x	Mag
VA locality													
VA11-H	x	x	—	ps	—	—	—	x	x	—	—	x	Py
VA11-J	x	x'	—	ps	x	x	—	x	x	—	—	x	Py
VA12-A	x	x'	—	ps	—	x'	x	x	x	—	x	x	Py
VA12-B	x	x	x'	ps	x	x	—	—	x	—	—	x	Mag

Note: ps = pseudomorphs after mineral observed; x = mineral present as primary phase; x' = mineral present as secondary phase; x'' = mineral present as primary and secondary phases; ? = identity not confirmed. Numerals indicate modal percentages. Mineral abbreviations are after Kretz (1983).

dominant S2 fabric is defined by aligned biotite and anthophyllite prisms, which enclose large poikiloblastic garnet typical of this assemblage. The large primary garnet grains contain quartz and magnetite but neither orthopyroxene nor orthoamphibole and are assumed to have grown early in the paragenetic sequence. A garnet sample from this assemblage yields a garnet growth age of 1201 m.y., as determined from Sm-Nd values obtained from the garnet and whole rock (Cornell et al., 1986). A second generation of garnet grows locally over biotite and orthoamphibole.

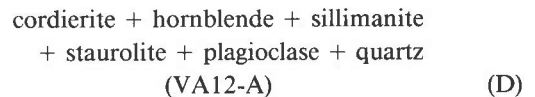
Assemblage C contains abundant retrograde staurolite euhedra on gedrite-cordierite and cordierite-cordierite grain boundaries (G2-D). In G5-B, these are intergrown, with gedrite replacing cordierite + plagioclase (Fig. 2B, 2C). G5-B contains primary gedrite and hornblende, as well as smaller grains of secondary gedrite. The earlier generation of gedrite is coarser and more equant than the later, retrograde, grains, many of which are fibrous or rhomb-shaped. Secondary garnet has grown over retrograde gedrite-staurolite intergrowths (Fig. 2D). In G2-D, sillimanite occurs with gedrite on cordierite grain boundaries, but it is unclear whether sillimanite and gedrite were stable together.

VA mineralization

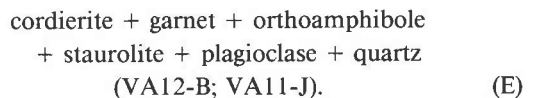
The VA mineralized zone (Fig. 1) is separated from the biotite gneisses of Smouspan by the Klipgatspan shear zone, 1 km wide. It lies along the strike from the Annex deposit, an uneconomic copper iron sulfide deposit whose pelitic wall rocks share a similar metamorphic history to those of the VA locality (Humphreys and Scheepers, 1993). The host sequence of both sulfide zones is similar and contains amphibolites, quartz-rich gneisses, biotite gneisses, and hornblende-biotite gneisses. Garnet-biotite thermometry from the Annex pelites indicates peak tem-

peratures of 580–620 °C (calibrations of Dasgupta et al., 1991, and Williams and Grambling, 1990, with corrections for Mn in garnet). A maximum pressure of 6.1 kbar (at 580 °C) is estimated from a single barometric calculation using the garnet-plagioclase-kyanite-quartz barometer of Powell and Holland (1988).

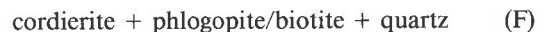
Amphibole-bearing assemblages occur in two bore holes, VA11 and VA12, and include:



and



In addition, VA12-A contains domains where the assemblage



was stable at the peak of metamorphism. Assemblage D (Fig. 3b) contains primary staurolite and sillimanite intergrown with rare grains of hornblende, surrounded partially by intergrowths of former cordierite and plagioclase. The occurrence of all five minerals together is restricted to the interface of domains containing Assemblages D and F. Hornblende is overgrown by sheaves of chlorite and subsequently by small grains of secondary staurolite (Fig. 2H), whereas cordierite has been replaced by varying proportions of staurolite, chlorite, quartz, and white mica (Fig. 2F). An outer rim of cloudy staurolite seen in Assemblage D is separated from the grain cores by a narrow band of quartz inclusions a few tens of micrometers from the grain boundary (Figs. 2G, 3b). This

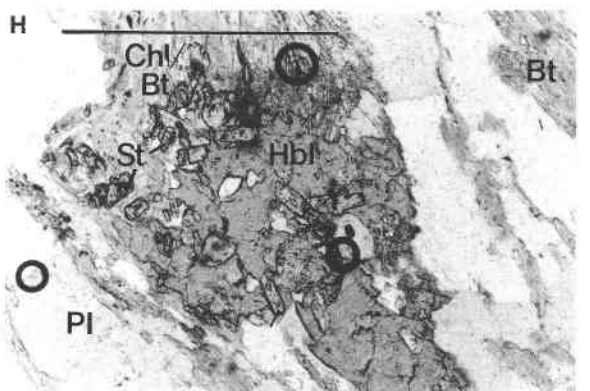
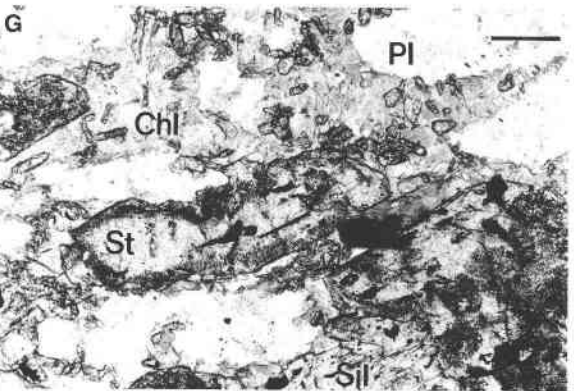
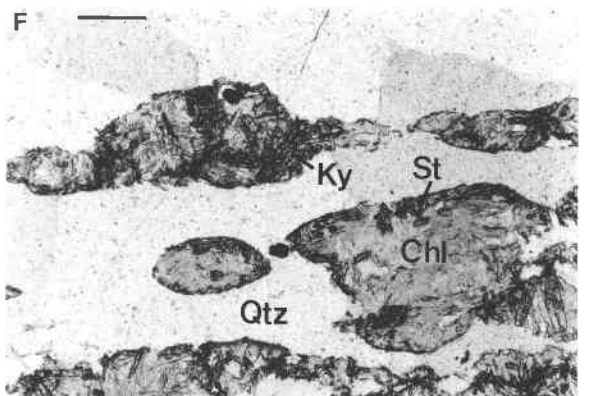
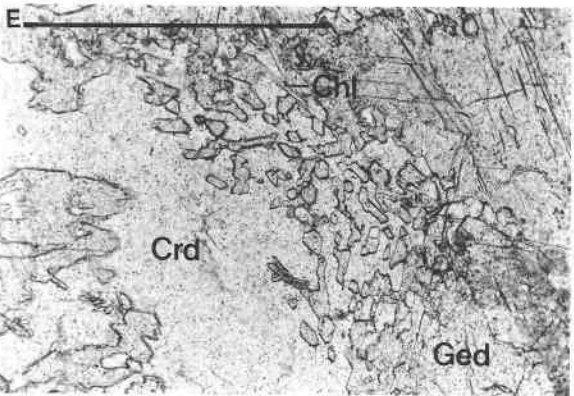
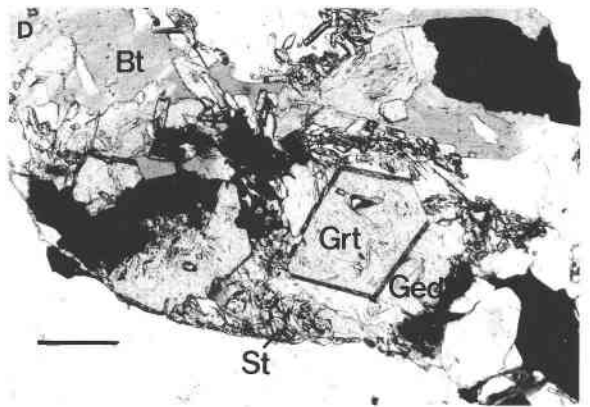
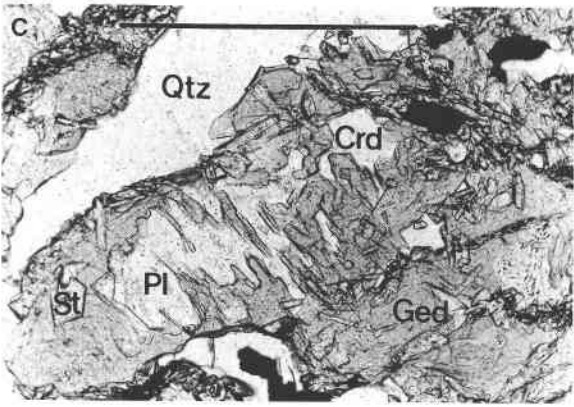
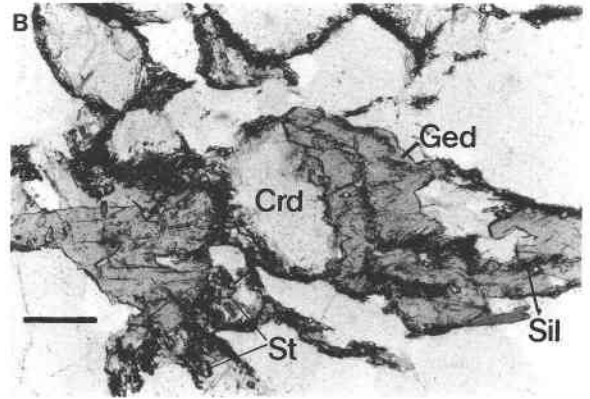
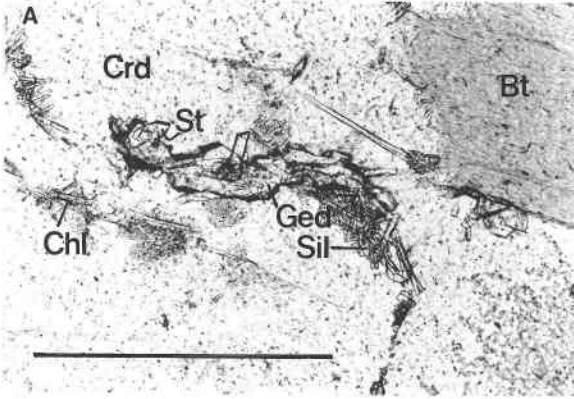


TABLE 2. Sequence of mineral parageneses

Kielder	Smouspan	VA mineralization
Primary assemblage		
Crd + Opx + Pl [± Grt, Hc, Qtz, Bt (rare)]	Crd + Oam + Pl + Qtz (± Grt, Hbl, Opx)	Crd + St ± Pl + Bt + Qtz (± Hbl, Sil, Oam, Grt)
Resultant assemblages on cooling/rehydration		
Oam + Chl	Oam + St	Ky + Chl + ?Ms
Sil + Oam	St + Chl	Chl + Qtz
Sil + St + Hbl	Sil + Chl	
St + Chl		
Minerals grown upon reheating		
Grt (on Oam + Bt)	Grt (on Oam + St)	Grt (on Chl + Bt) St (on Chl + Bt + Hbl)

rim is resorbed against chlorite and thus predates the growth of secondary staurolite, which grew subsequently across chlorite and hornblende (Table 2).

In Assemblage E, primary garnet is intergrown with gedrite and staurolite; patches of fine-grained secondary micas, staurolite, and quartz indicate the former existence of cordierite in the peak assemblage. The first generation of garnet was locally replaced by chlorite before a second generation of garnet formed as a rim upon the resorbed garnet cores.

Cordierite in Assemblage F has broken down to form acicular grains of kyanite, together with staurolite and chlorite. This is a key petrogenetic indicator and is correlated with the retrograde growth of kyanite after sillimanite in the Annex pelites (Humphreys and Scheepers, 1993).

MINERAL COMPOSITIONS

Minerals were analyzed on a Cameca Camebax electron probe microanalyzer housed at the Department of Geochemistry, University of Cape Town. Accelerating

←

Fig. 2. Photomicrographs of textures from amphibole-bearing aluminous gneisses occurring in the Copperton Formation. Scale bars = 0.5 mm. (A) Replacement of cordierite (Crd) by sillimanite (Sil), chlorite (Chl), and gedrite (Ged): KDH5-105. (B) Replacement of cordierite (Crd) by gedrite (Ged) and staurolite (St); fibrous sillimanite also occurs on grain boundaries: G2-D. (C) Alteration of plagioclase (Pl) and cordierite to gedrite and staurolite; gedrite has grown along plagioclase twin planes: G5-B. (D) Regrowth of euhedral garnet (Grt) upon a gedrite-staurolite substrate: G5-B. (E) Euhedral grains of orthoamphibole (Ged) resulting from the breakdown of cordierite + orthopyroxene: KDH5-105. (F) Alteration of cordierite to kyanite (Ky), chlorite (Chl), and quartz (Qtz); staurolite (St) appears to have grown later from chlorite: VA12-A. (G) Intergrowth of sillimanite (Sil) and staurolite (St); staurolite has cloudy poikiloblastic margins and is replaced by chlorite and biotite in the center of the photograph: VA12-A. (H) Hornblende porphyroblast (Hbl) with margins corroded by chlorite (Chl) and biotite (Bt) and subsequently overgrown by staurolite (St): VA12-A.

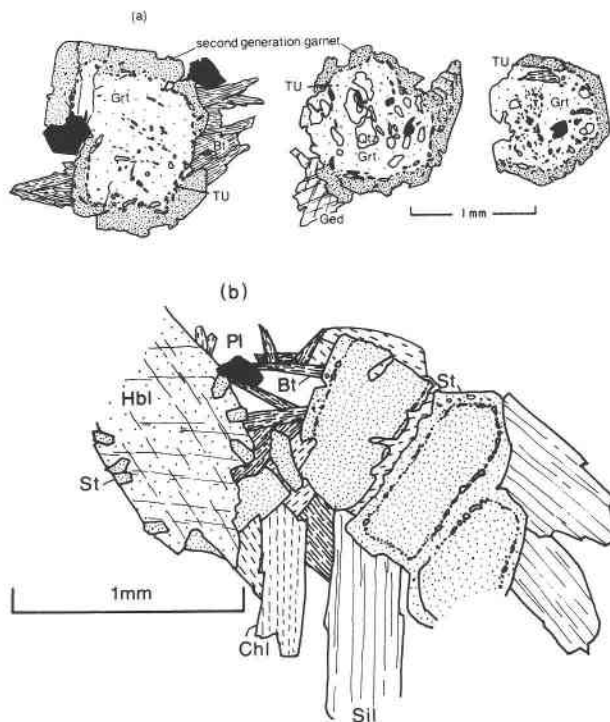


Fig. 3. Line drawings of textures in amphibole-bearing rocks: (a) Overgrowths of second-generation garnet upon preexisting cores in samples VA12-B (left) and G5-B (center, right). TU is the textural unconformity that represents the hiatus caused by resorption of the core prior to overgrowth of the rim. (b) Stable assemblage of staurolite, sillimanite, and staurolite in VA12-A.

potential was 15 kV, with a beam current of 20 nA for feldspars and sheet silicates or 40 nA for other minerals. Raw data were reduced using the method of Bence and Albee (1968). Mineral analyses are listed in Tables 3–8. The projection of mineral compositions from quartz, albite, and H_2O is shown in Figure 4.

Garnet

Kielder. Zoned garnet from the orthoamphibole-rich band in KDH5-420 has an outer rim that is distinct chemically and optically from the interior. A central core shows increasing X_{Mg} toward 0.35 at the inner rim, which is succeeded by a decrease in the outer rim to 0.23. The opposite effect is seen in X_{Fe} . X_{Ca} is asymmetric, reflecting X_{Mg} on one limb and X_{Fe} on the other; X_{Mn} increases to both rims (Fig. 5A), indicating partial resorption of the core before the rim grew.

Smouspan. Garnets in Assemblages B and C have broadly similar profiles, characterized by flat cores, increasing X_{Mg} toward the rims, and a decrease at the outer parts of the garnet (Fig. 5B). X_{Fe} varies in an inverse manner to X_{Mg} , whereas X_{Mn} and X_{Ca} profiles vary nonsystematically. In G5-B, X_{Ca} is constant in the core before decreasing at the extreme edge and is broadly mirrored by variations in X_{Mn} , which increase from near the mar-

TABLE 3. Representative mineral analyses of garnet

	KDH5-420		SM7-82		SP2-B	G5-B		VA12-B	
	Core	Rim	Core	Rim	Core	Core	Rim	Core	Rim
SiO ₂	38.65	37.96	37.55	38.05	38.24	37.42	37.59	36.96	37.03
Al ₂ O ₃	22.48	22.14	21.75	21.98	22.01	21.75	21.98	21.19	21.26
FeO	27.06	30.50	29.91	33.29	30.71	32.74	33.12	29.31	28.02
MnO	1.92	2.85	4.33	2.38	2.08	1.67	1.46	6.13	7.59
MgO	8.68	6.08	4.38	5.03	6.14	5.12	4.64	3.22	4.19
CaO	2.81	1.87	3.28	1.30	2.47	2.45	2.65	4.61	2.52
Total	101.60	101.40	101.20	102.03	101.65	101.15	101.44	101.42	100.61
Si	2.950	2.956	2.960	2.972	2.968	2.947	2.954	2.940	2.957
Al	2.022	2.032	2.020	2.023	2.013	2.019	2.035	1.986	2.001
Fe	1.727	1.986	1.972	2.175	1.994	2.157	2.176	1.949	1.871
Mn	0.124	0.188	0.289	0.158	0.137	0.111	0.097	0.413	0.513
Mg	0.987	0.706	0.515	0.585	0.710	0.601	0.543	0.382	0.499
Ca	0.230	0.156	0.277	0.109	0.206	0.207	0.223	0.393	0.215
Total	8.040	8.024	8.033	8.022	8.028	8.042	8.028	8.063	8.056
Mg/(Mg + Fe)	0.364	0.262	0.207	0.212	0.286	0.218	0.200	0.164	0.211

Note: atomic proportions calculated on the basis of 12 O atoms.

gin to the extreme rim. The variation in zoning pattern in these garnets supports the existence of a secondary rim, which is indicated by inclusion patterns and optical observations (cf. Figs. 3a, 5B).

VA mineralization. Garnet from VA12-B has a spessartine component, which increases from $X_{Mn} = 0.14$ at the core to 0.23 at the interface between primary and secondary garnet and drops to 0.17 at the outer rim. The high X_{Mn} at the interface is interpreted as the result of resorption of primary garnet during retrogression to biotite and chlorite. The decrease to the rims reflects the normal fractionation of Mn in garnet and is interpreted as an indication of prograde growth of secondary garnet.

X_{Mg} increases from 0.11 (core) to 0.17 (rim) with no hiatus at the primary-secondary interface (Fig. 5C).

Amphibole

In this paper, all amphiboles with cations over 15 pfu (23 O atoms) in the M4, octahedral, and tetrahedral sites have been corrected for Fe³⁺. Orthoamphiboles have been subjected to minimum Fe³⁺ corrections, whereas hornblende structural formulae are given as the mean of the minimum and maximum Fe³⁺ corrections recommended by Schumacher (1991). Compositions of orthoamphiboles are summarized in Figure 6 and indicate (1) a positive correlation between ⁶³Al and Na_{tot} (Fig. 6a, 6b) and

TABLE 4. Mineral analyses of orthoamphiboles

	Kielder									
	KDH5-420		KDH5-105				KDH5-105			
	Cores		Cores		Cores		Rims		Rims	
SiO ₂	50.14	50.00	54.92	54.86	54.57	42.50	43.88	50.43	47.16	
TiO ₂	0.08	0.08	nd	nd	nd	0.10	nd	nd	nd	
Al ₂ O ₃	8.25	8.30	2.31	2.47	1.93	20.29	18.82	8.90	13.56	
FeO	19.37	19.69	17.59	17.74	17.92	19.18	17.92	18.25	17.52	
MnO	0.71	0.70	1.31	1.47	1.43	1.55	1.49	1.44	1.38	
MgO	18.97	18.68	21.82	21.46	21.64	14.04	15.03	18.55	17.80	
CaO	0.38	0.41	0.28	0.27	0.26	0.37	0.41	0.32	0.34	
Na ₂ O	0.90	0.95	0.11	0.16	0.09	2.17	1.86	0.78	1.12	
Total	98.80	98.81	98.34	98.43	97.84	100.20	99.41	98.67	98.88	
Si	7.135	7.130	7.751	7.753	7.753	6.043	6.243	7.174	6.683	
⁴¹ Al	0.865	0.870	0.249	0.247	0.247	1.957	1.757	0.826	1.317	
Total	8.000	8.000	8.000	8.000	8.000	8.000	8.000	8.000	8.000	
⁶³ Al	0.519	0.524	0.094	0.164	0.076	1.443	1.398	0.667	0.948	
Ti	0.008	0.008	—	—	—	0.010	—	—	—	
Fe ³⁺	0.083	0.001	0.138	0.074	0.145	—	—	—	0.061	
Mg	4.024	3.971	4.590	4.520	4.583	2.977	3.188	3.932	3.759	
Fe ²⁺	0.366	0.496	0.178	0.242	0.196	0.570	0.414	0.401	0.232	
Total	5.000	5.000	5.000	5.000	5.000	5.000	5.000	5.000	5.000	
Fe ²⁺	1.856	1.851	1.760	1.781	1.788	1.710	1.718	1.770	1.783	
Mn	0.085	0.085	0.156	0.176	0.172	0.186	0.180	0.173	0.165	
Ca	0.058	0.063	0.042	0.042	0.040	0.057	0.063	0.049	0.052	
Na	0.001	0.001	0.031	0.001	—	0.047	0.039	0.008	—	
Total	2.000	2.000	1.989	2.000	2.000	2.000	2.000	2.000	2.000	
Na	0.247	0.262	—	0.042	0.026	0.553	0.473	0.208	0.308	
Total	0.247	0.262	0.000	0.042	0.026	0.553	0.473	0.208	0.308	
Mg/(Mg + Fe)	0.644	0.628	0.703	0.691	0.698	0.566	0.599	0.644	0.651	

TABLE 4.—Continued

	Smouspan												
	SP2-B		SM7-82		G2-D								
	Core		Cores		Core	(profile)	Rim						
SiO ₂	47.33		47.03		46.66		44.53		44.13		46.39		44.40
TiO ₂	0.42		0.15		0.28		0.18		0.16		0.10		0.14
Al ₂ O ₃	10.96		11.03		11.04		17.62		18.08		15.65		17.86
FeO	25.43		24.81		25.18		19.38		19.15		18.73		18.88
MnO	0.55		0.69		0.70		2.18		2.16		2.03		2.23
MgO	14.10		14.64		14.00		14.26		14.16		14.98		14.28
CaO	0.38		0.27		0.41		0.44		0.45		0.37		0.45
Na ₂ O	1.18		1.35		1.36		1.67		1.75		1.34		1.67
Total	100.35		99.97		99.63		100.26		100.04		99.59		99.91
Si	6.846		6.810		6.807		6.327		6.282		6.589		6.317
¹⁴ Al	1.154		1.190		1.193		1.673		1.718		1.411		1.683
Total	8.000		8.000		8.000		8.000		8.000		8.000		8.000
¹⁶ Al	0.714		0.696		0.705		1.277		1.316		1.209		1.312
Ti	0.045		0.016		0.031		0.019		0.018		0.011		0.015
Fe ³⁺	0.034		0.098		0.037		—		—		—		—
Mg	3.040		3.160		3.043		3.021		3.004		3.171		3.028
Fe ²⁺	1.167		1.030		1.184		0.683		0.662		0.609		0.645
Total	5.000		5.000		5.000		5.000		5.000		5.000		5.000
Fe ²⁺	1.875		1.877		1.851		1.620		1.617		1.616		1.602
Mn	0.066		0.083		0.085		0.262		0.260		0.244		0.269
Ca	0.059		0.040		0.064		0.067		0.068		0.056		0.068
Na	—		—		—		0.051		0.055		0.084		0.061
Total	2.000		2.000		2.000		2.000		2.000		2.000		2.000
Na	0.331		0.379		0.385		0.408		0.428		0.285		0.400
Total	0.331		0.379		0.385		0.408		0.428		0.285		0.400
Mg/(Mg + Fe)	0.500		0.521		0.501		0.568		0.569		0.588		0.574

	VA locality								
	G5-B				VA12-B				
	Core		(profile)		Rim		Cores		Rim
SiO ₂	41.16	42.32	42.82	42.66	43.19	44.21	47.76	48.95	53.17
TiO ₂	0.16	0.13	0.09	0.10	0.10	0.11	0.14	0.13	0.08
Al ₂ O ₃	20.99	20.19	19.02	19.32	18.92	17.72	10.42	7.97	3.54
FeO	23.43	23.38	23.00	22.79	23.04	22.69	20.74	20.61	20.50
MnO	0.35	0.31	0.31	0.34	0.30	0.37	1.63	1.75	1.52
MgO	12.11	12.54	12.77	12.76	12.71	13.33	16.87	17.84	20.03
CaO	0.41	0.43	0.43	0.35	0.40	0.44	0.54	0.45	0.34
Na ₂ O	2.28	2.15	1.86	1.84	1.88	1.61	1.29	0.98	0.41
Total	100.89	101.45	100.30	100.16	100.54	100.48	99.39	98.68	99.59
Si	5.908	6.025	6.149	6.126	6.182	6.312	6.849	7.043	7.520
¹⁴ Al	2.092	1.975	1.851	1.874	1.818	1.688	1.151	0.957	0.480
Total	8.000	8.000	8.000	8.000	8.000	8.000	8.000	8.000	8.000
¹⁶ Al	1.458	1.413	1.368	1.396	1.374	1.294	0.610	0.395	0.110
Ti	0.018	0.014	0.013	0.011	0.010	0.012	0.015	0.015	0.009
Fe ³⁺	—	—	—	—	—	—	0.151	0.260	0.240
Mg	2.591	2.661	2.705	2.731	2.712	2.836	3.607	3.827	4.222
Fe ²⁺	0.933	0.912	0.914	0.862	0.904	0.858	0.617	0.503	0.419
Total	5.000	5.000	5.000	5.000	5.000	5.000	5.000	5.000	5.000
Fe ²⁺	1.880	1.872	1.822	1.876	1.854	1.851	1.720	1.717	1.766
Mn	0.043	0.037	0.038	0.041	0.036	0.044	0.197	0.214	0.182
Ca	0.062	0.065	0.070	0.054	0.061	0.068	0.083	0.069	0.052
Na	0.015	0.026	0.070	0.029	0.049	0.037	—	—	—
Total	2.000	2.000	2.000	2.000	2.000	2.000	2.000	2.000	2.000
Na	0.620	0.567	0.457	0.485	0.474	0.408	0.360	0.272	0.112
Total	0.620	0.567	0.457	0.485	0.474	0.408	0.360	0.272	0.112
Mg/(Mg + Fe)	0.479	0.489	0.497	0.499	0.496	0.512	0.607	0.634	0.659

Note: atomic proportions on the basis of 23 O atoms; minimum Fe³⁺ correction employed; nd = not determined.

(2) a negative correlation between ¹⁶Al and Mg/(Mg + Fe) calculated with a minimum Fe³⁺ correction (Fig. 6b, 6c). Figure 6a illustrates the separation of orthoamphibole compositions into two fields—those in rocks dominated by secondary growth of staurolite and sillimanite and those that have clearly derived from orthopyroxene

[SP2-B, SM7-82, KDH5-420, and KDH5-105 (cores only)]. The exception is VA12-B, which strictly belongs to neither of these groups. The best interpretation of these data is that they reflect variation in bulk composition.

Kielder. The cores of the large anthophyllite grains that replaced orthopyroxene in KDH5-105 have minor

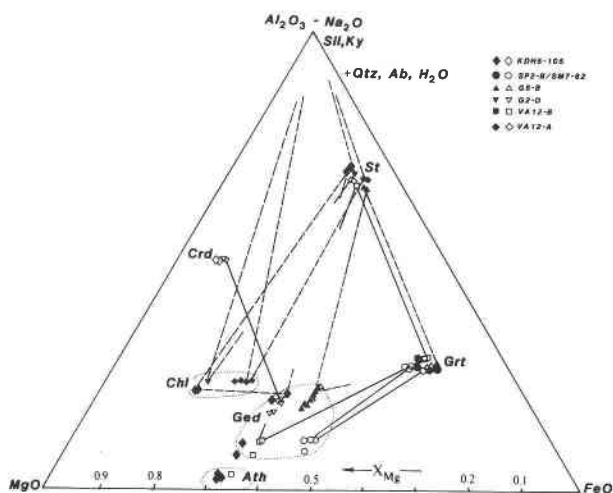


Fig. 4. Projection of mineral compositions from albite, quartz, and H₂O. Compositions of orthoamphibole have not been corrected for Fe³⁺. Open symbols are prograde minerals; closed symbols are retrograde minerals.

amounts of ⁶¹Al (0.094–0.164 pfu) and Na (0.026–0.042 pfu), whereas the rims are richer in both (⁶¹Al = 0.667–1.443 pfu; Na = 0.216–0.600 pfu). Rims are less magnesian [Mg/(Mg + Fe) = 0.57–0.64] than the cores [Mg/(Mg + Fe) = 0.69–0.71]. Hornblende that rims antho-

TABLE 5. Mineral analyses of hornblende

	KDH5-105		G5-B		VA12-A	
	Rim	Core	Rim	Core	Rim	Core
SiO ₂	43.59	42.65	42.38	42.82	42.28	
TiO ₂	0.23	0.28	0.32	0.44	0.36	
Al ₂ O ₃	17.18	18.16	17.98	16.87	17.09	
FeO	14.19	17.32	17.47	15.87	15.81	
MnO	0.62	0.15	0.17	0.92	0.90	
MgO	11.01	9.23	9.22	10.44	10.28	
CaO	10.92	10.83	10.77	10.14	10.28	
Na ₂ O	1.59	1.70	1.70	1.86	1.81	
K ₂ O	0.16	0.23	0.24	0.16	0.16	
Total	99.49	100.55	100.25	99.41	98.97	
Si	6.181	6.063	6.045	6.112	6.065	
⁶¹ Al	1.819	1.937	1.955	1.888	1.935	
Total	8.000	8.000	8.000	8.000	8.000	
⁶¹ Al	1.052	1.107	1.068	0.950	0.954	
Ti	0.024	0.030	0.034	0.028	0.039	
Fe ³⁺	0.616	0.634	0.684	0.857	0.814	
Mg	2.326	1.955	1.960	2.222	2.198	
Fe ²⁺	0.982	1.274	1.254	0.943	0.995	
Total	5.000	5.000	5.000	5.000	5.000	
Fe ²⁺	0.085	0.152	0.146	0.082	0.088	
Mn	0.075	0.018	0.020	0.112	0.109	
Ca	1.660	1.650	1.645	1.550	1.580	
Na	0.180	0.180	0.189	0.256	0.223	
Total	2.000	2.000	2.000	2.000	2.000	
Na	0.256	0.289	0.281	0.258	0.280	
K	0.029	0.041	0.043	0.030	0.031	
Total	0.285	0.330	0.324	0.288	0.311	
Mg/(Mg + Fe)	0.709	0.578	0.583	0.684	0.613	

Note: atomic proportions calculated on the basis of 23 O atoms; Fe³⁺ calculated from the mean of minimum and maximum Fe³⁺ corrections.

TABLE 6. Mineral analyses of cordierite

	KDH5-420	KDH5-105	G2-D		
SiO ₂	49.04	49.06	49.20	47.86	48.34
Al ₂ O ₃	33.64	33.42	33.47	33.05	33.11
FeO	4.65	3.67	3.91	3.80	3.84
MnO	0.14	0.20	0.25	0.30	0.31
MgO	10.46	10.37	10.36	9.65	9.80
Na ₂ O	0.15	0.57	0.60	0.85	0.89
Total	98.08	97.29	97.79	95.51	96.29
Si	4.988	5.007	5.003	4.986	4.998
Al	4.026	4.020	4.011	4.058	4.035
Fe	0.395	0.314	0.333	0.332	0.332
Mn	0.012	0.018	0.021	0.027	0.027
Mg	1.583	1.577	1.571	1.499	1.511
Na	0.029	0.113	0.119	0.173	0.180
Total	11.033	11.049	11.058	11.075	11.083
Mg/(Mg + Fe)	0.800	0.834	0.825	0.819	0.820

Note: atomic proportions on the basis of 18 O atoms.

phyllite is a ferroan pargasite and more magnesian than its host orthoamphibole [Mg/(Mg + Fe)_{Hbl} = 0.71].

Smouspan. Orthoamphiboles from Assemblage B are less aluminous than gedrite in Assemblage C but show a strong depletion in Na and ⁶¹Al near their rims, accompanied by an increase in Mg/(Fe + Mg). In Assemblage C, gedrite is strongly zoned (Fig. 6b). Although there is some heterogeneity, rims of primary orthoamphibole in G5-B are enriched in Mg and depleted in Na and Al. Hornblende is more magnesian [Mg/(Mg + Fe) = 0.58] than coexisting orthoamphibole.

VA locality. Analyses of orthoamphibole in VA12-B show an increase in Mg/(Mg + Fe) and a decrease in Na and ⁶¹Al from core to rim. Hornblende in VA12-A (Assemblage D) is ferroan pargasite with minor enrichment in Fe and Al at the rim.

Cordierite

At Kielder, cordierite analyses range in Mg/(Mg + Fe) from 0.70 to 0.84. The most Mg-rich analyses are from KDH5-105, where cordierite was replaced by gedrite, sillimanite, and staurolite. In KDH5-420, cordierite in the unaltered Assemblage A is less magnesian than that in the orthoamphibole-rich band. This results directly from a continuous shift in Mg/(Mg + Fe)_{Crd} to higher values as it loses Fe to reaction products with lower Mg/(Mg + Fe). In the Smouspan samples, fresh cordierite in G2-D [Mg/(Mg + Fe) = 0.82] has a Mg/(Mg + Fe) ratio similar to a heavily pinitized replacement in G5-B. The latter has Al/Si ratios similar to cordierite, but a substantially lower total (Humphreys, 1991).

Staurolite

Four analyses from KDH5-105 (Kielder) average 0.51 wt% ZnO and span a range in Mg/(Mg + Fe) of 0.22–0.24. At Smouspan, staurolite from Assemblage C is Zn-free, with Mg/(Mg + Fe) in the range 0.22–0.25. Minor amounts of TiO₂ and MnO are present. In VA12-A, primary and secondary staurolite have Mg/(Mg + Fe) = 0.23–0.24 in Assemblage D, whereas secondary staurolite

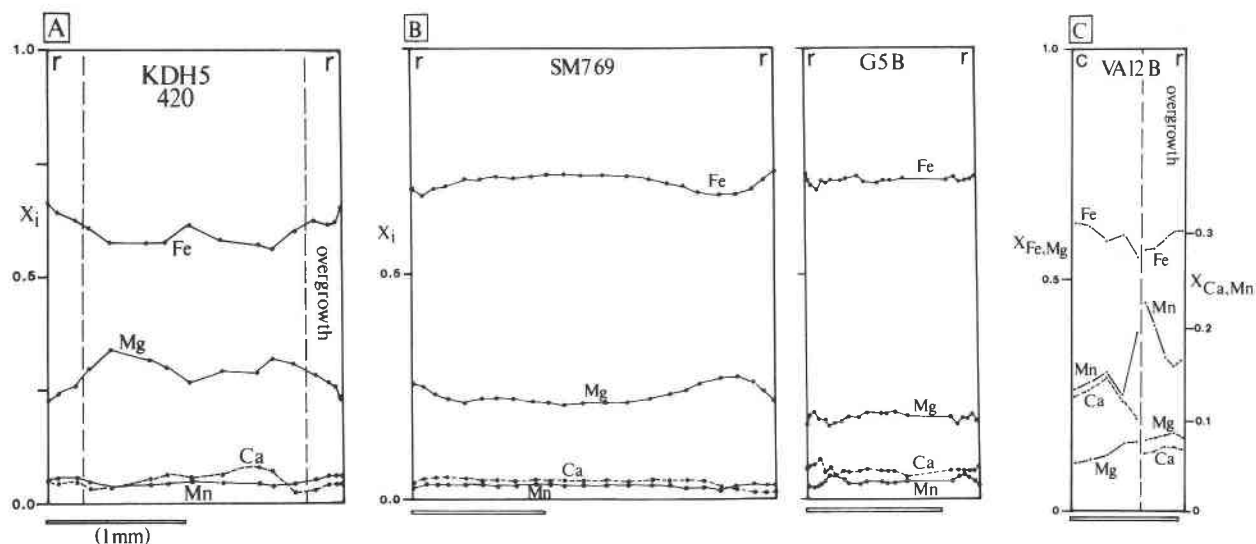


Fig. 5. Compositional profiles in garnet: (A) KDH5-420 (Kielder); (B) SM7-69 and G5-B (Smouspan); (C) VA12-B (VA mineralization). Values are ratios of the individual elements divided by the sum of Mg + Fe + Ca + Mn.

in Assemblage F has $Mg/(Mg + Fe)$ values of 0.17–0.18. In addition, the former is Zn-free, whereas staurolite after cordierite in Assemblage F is mildly zincian. Staurolite in VA12-B is zincian with $Mg/(Mg + Fe) = 0.25$.

Plagioclase

Variations in X_{An} are found in all three localities. At Kielder, the range in X_{An} is small, between 0.29 and 0.31. At Smouspan, Assemblage B has a range of 0.24–0.28, whereas Assemblage C has a range of 0.45–0.48; this difference results from bulk composition. The two VA samples have ranges in X_{An} of 0.35 (core) to 0.41 (rim) in VA12-A and 0.38 (core) to 0.36 (rim) in VA12-B. The greater variation in VA12-A is possibly a result of Ca enrichment due to the breakdown of hornblende in the rock during retrogression.

Chlorite

All chlorite in the samples described resulted from retrogression of orthopyroxene, orthoamphibole, cordierite, garnet, staurolite, or biotite. All are magnesian ferroan clinocllore. $Mg/(Mg + Fe)$ in KDH5-105 (Kielder) is 0.78, midway between that of cordierite and biotite. A single chlorite sample from G2-D (Smouspan) has $Mg/(Mg + Fe) = 0.75$ and is more Fe-rich than cordierite in the same sample. At the VA locality, $Mg/(Mg + Fe)_{Chl}$ lies between 0.65 and 0.66 for Assemblage D (chlorite derived from biotite and cordierite) and between 0.67 and 0.69 for Assemblage F (derived from cordierite alone).

Since $Mg/(Mg + Fe)_{Crd} > Mg/(Mg + Fe)_{Chl}$, the alteration of cordierite to chlorite + staurolite in all three localities was accompanied by the breakdown of a suit-

TABLE 7. Mineral analyses of staurolite

	KDH5-105		G2-D	G5-B	VA12-A		VA12-B
SiO ₂	28.63	28.68	28.09	27.92	28.39	27.87	27.84
TiO ₂	0.47	0.24	0.58	0.44	0.47	0.57	0.62
Al ₂ O ₃	54.69	54.71	52.86	52.41	53.93	53.66	53.10
FeO	11.44	11.14	12.39	13.96	12.97	13.45	13.56
MnO	0.37	0.51	0.60	nd	0.57	0.61	0.48
MgO	1.85	2.02	2.13	2.46	1.54	2.37	2.58
ZnO	0.51	0.48	nd	nd	0.31	nd	0.30
Total	97.96	97.78	96.65	97.25	98.18	98.53	98.48
Si	3.756	3.767	3.756	3.739	3.747	3.676	3.683
Ti	0.047	0.024	0.058	0.044	0.046	0.057	0.062
Al	8.457	8.468	8.331	8.272	8.389	8.342	8.280
Fe	1.255	1.224	1.386	1.584	1.431	1.484	1.501
Mn	0.041	0.057	0.068	—	0.064	0.068	0.054
Mg	0.362	0.396	0.425	0.490	0.303	0.467	0.508
Zn	0.050	0.046	—	—	0.031	—	0.030
Total	13.968	13.982	14.024	14.117	14.011	14.094	14.118
Mg/(Mg + Fe)	0.224	0.244	0.235	0.236	0.175	0.239	0.253

Note: atomic proportions on the basis of 22 O atoms; nd = not determined.

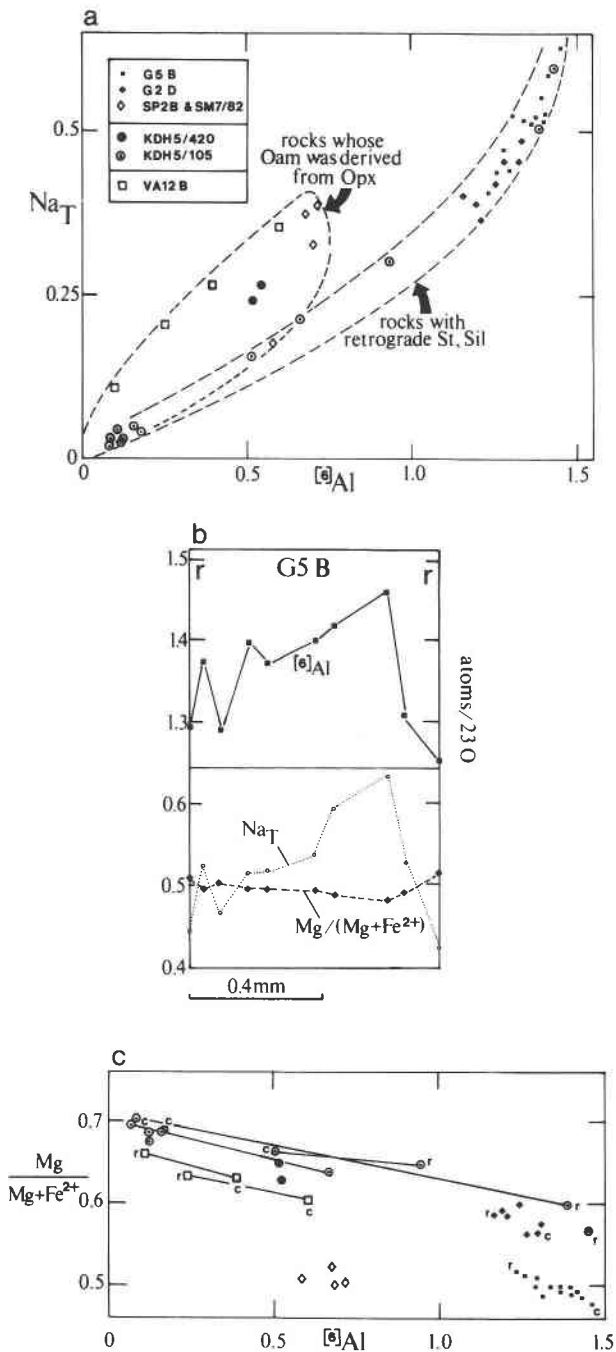


Fig. 6. Mineral chemistry of orthoamphiboles: (a) Plot of Na_{tot} vs. $[Al]$ (per formula unit of 23 O atoms). All analyses have been corrected for Fe^{3+} using a minimum Fe^{3+} correction. (b) Zoning profile across a primary gedrite from G5-B. (c) Plot of $Mg/(Mg + Fe)$ against $[Al]$ (per formula unit).

able Fe-rich mineral, either amphibole or (more probably) biotite, depending upon the original mineralogy.

REACTION HISTORY AND PHASE RELATIONSHIPS

Seven of the above samples contained cordierite and an amphibole at the metamorphic peak, whereas a further

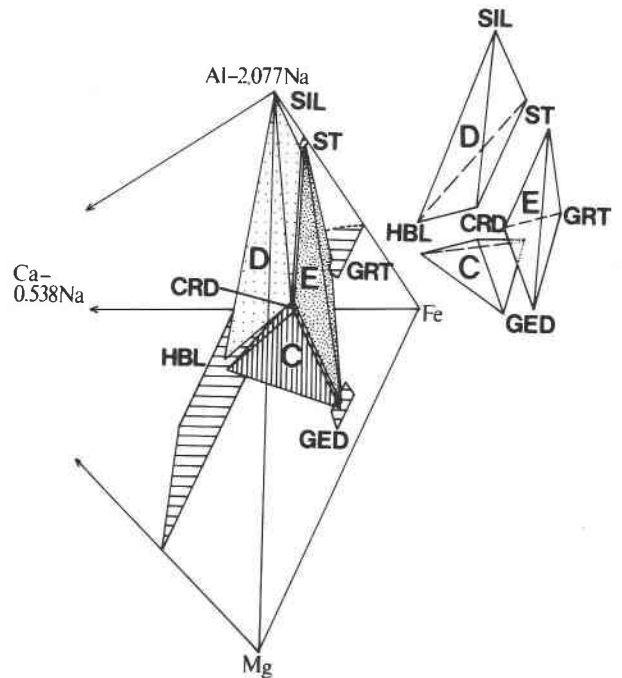


Fig. 7. Quaternary projection of the prograde amphibolite facies Assemblages C, D, and E from An_{35} , quartz, and vapor (Spear, 1977). Note that garnet, being slightly calcic, is projected within the tetrahedron, so that the garnet-cordierite tie line in Assemblages C and E passes behind the staurolite-gedrite tie line, which is in the front face of the tetrahedron. The exploded diagram on the right clarifies these relationships and shows that the three assemblages form interlocking (and hence compatible) tetrahedra in this projection.

five contain the nondiagnostic Assemblage B (orthoamphibole + garnet + plagioclase + biotite + quartz), and are not discussed further. The useful prograde parageneses can be summarized as follows:

- garnet + orthopyroxene + cordierite (A)
- garnet + hornblende + orthoamphibole + cordierite (C)
- staurolite + hornblende + sillimanite + cordierite (D)
- staurolite + garnet + orthoamphibole + cordierite. (E)

All assemblages coexist with plagioclase + quartz, whereas biotite is present in Assemblages C, D, and E. These three assemblages can be represented in projection from plagioclase (An_{35}), quartz, and vapor (Fig. 7). This suggests that Assemblages C, D, and E all represent peak amphibolite facies assemblages formed at similar pressures and temperatures in rocks of slightly different bulk composition.

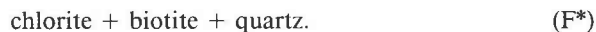
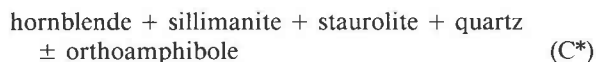
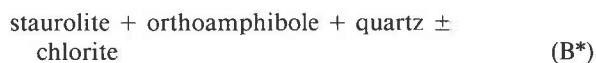
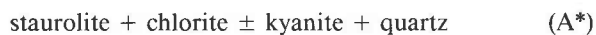
Retrograde parageneses are subassemblages of the total list of retrograde minerals in a given rock. They are placed together on the evidence of spatial proximity along grain

TABLE 8. Mineral analyses of plagioclase

	KDH5-420	KDH5-105	SP2-B	SM7-82	G2-D	G5-B	VA12-A		VA12-B
							Core	Rim	
SiO ₂	59.09	61.65	62.40	62.82	56.07	56.54	58.36	58.43	60.19
Al ₂ O ₃	25.99	23.73	23.40	23.07	26.19	25.91	25.73	25.54	24.63
CaO	8.05	6.22	5.84	5.22	9.81	9.35	6.82	8.51	7.30
Na ₂ O	6.73	8.14	8.28	8.88	5.88	6.19	6.40	6.72	7.14
K ₂ O	0.05	nd	0.09	0.09	nd	nd	1.10	nd	nd
Total	99.91	99.74	100.01	100.08	97.95	97.99	98.63	99.20	99.26
Si	2.640	2.748	2.769	2.781	2.570	2.591	2.644	2.638	2.697
Al	1.369	1.246	1.224	1.204	1.415	1.399	1.374	1.359	1.301
Ca	0.385	0.297	0.278	0.248	0.482	0.459	0.331	0.412	0.350
Na	0.583	0.704	0.712	0.762	0.522	0.550	0.562	0.588	0.620
K	0.003	—	0.005	0.005	—	—	0.064	—	—
Total	4.980	4.995	4.988	5.000	4.989	4.999	4.975	4.997	4.968
X _{An}	0.396	0.297	0.279	0.244	0.480	0.455	0.346	0.412	0.361

Note: atomic proportions on the basis of eight O atoms; nd = not determined.

boundaries or because they constitute a pseudomorph (for example after cordierite):



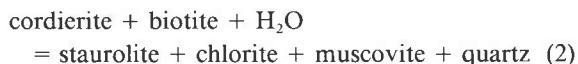
The reactions that link prograde and retrograde assemblages involve transitions from the stability fields of orthopyroxene, cordierite, hornblende, and sillimanite to those of staurolite, chlorite, and kyanite. Although the detail of each reaction differs, these transitions in broad terms involve a movement from lower pressures and higher temperatures to conditions of lower temperature along a near-isobaric P - T trajectory.

Interpretation of textures in rocks without hornblende

The following reactions are interpreted from the textural evidence in samples either with a single orthoamphibole or no amphibole at all. The widespread replacement of cordierite can be described by the reaction

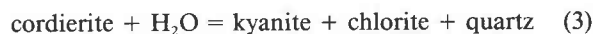


but is problematical because chlorite and staurolite are both less magnesian than the reactant cordierite. The texture is better represented by the KFMASH univariant reaction

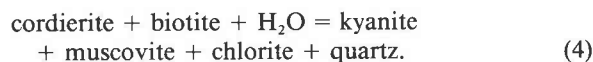


which is supported by biotite inclusions in cordierite pseudomorphs and random flakes of white mica interlay-

ered with chlorite in VA12-A. Pseudomorphing of cordierite by kyanite-bearing assemblages in the same sample can be described by the analogous reactions:



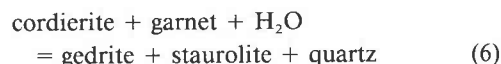
and



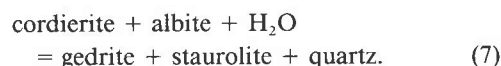
The alteration of cordierite to gedrite in G5-B is described by



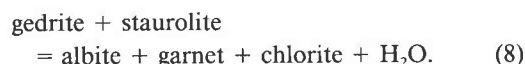
and the univariant reaction



which produce intergrowths of staurolite and gedrite along the grain boundaries of cordierite. Locally, twinned plagioclase is replaced by veinlets of gedrite and staurolite euhedra on the grain boundaries and is described by



In VA12-B (Assemblage E), the opposite reaction is inferred from the corona growth of plagioclase from primary staurolite:



At Kielder, the local coexistence of gedrite and sillimanite as small grains along grain boundaries of cordierite may be due to the reaction



This is usually regarded as a higher pressure assemblage (Harley, 1985; Visser and Senior, 1990), with kyanite

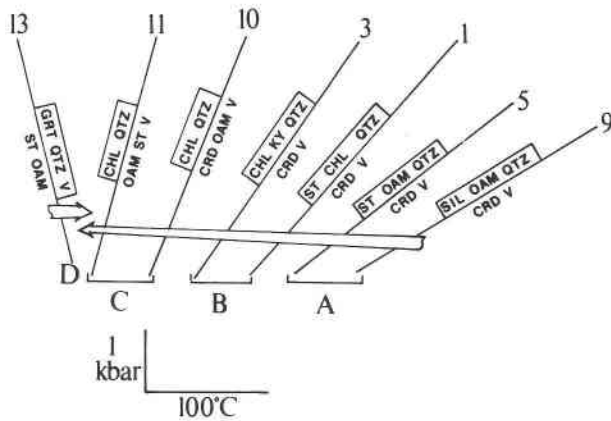
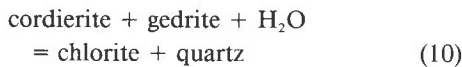


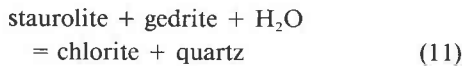
Fig. 8. Slopes of continuous reactions in FMASH predicted from the Holland and Powell (1990) data set. Products of reactions interpreted to have occurred on textural grounds are in boxes. See text for discussion.

commonly being the stable aluminum silicate, although Hudson and Harte (1985) place the reaction at 4–6 kbar.

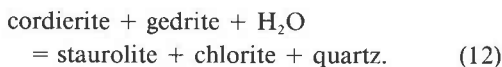
In Smouspan samples G2-D and G5-B, chlorite sheaves have grown across other retrograde products. This final stage of rehydration can be described in the FMASH continuous reactions



and

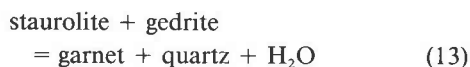


and the univariant FMASH reaction

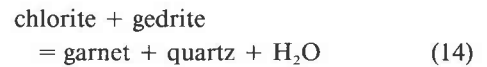


Reactions that are continuous in FMASH (Reactions 1, 3, 5, 9, 10, 11) have been plotted to scale in Figure 8 to illustrate the constraints placed upon the retrograde path. Predictably, the reactions involving chlorite require a proportionately higher molar quantity of H_2O and thus have steeper slopes. Reactions interpreted to have occurred last in the retrograde sequence (Reactions 10 and 11) have the steepest slopes of all. Although chlorite-producing reactions place little constraint upon the retrograde path, the shallower reactions (Reactions 5 and 9) are consistent with an isobaric cooling path.

In all three localities, the regrowth of garnet from gedrite + staurolite (G5-B), gedrite + chlorite (VA12-B), or anthophyllite + biotite (KDH5-420, V55-1050) is interpreted as a later prograde metamorphic event. The slopes of the relevant FMASH reactions



and

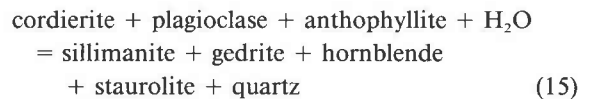


are negative, necessitating a shift to higher temperature to produce garnet from the hydrous reactants. It is clear that garnet cannot be produced along the same P - T vector that produced staurolite, chlorite, and gedrite from cordierite (Fig. 8).

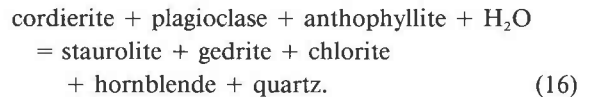
Interpretation of textures in rocks with hornblende

Prograde hornblende-bearing assemblages (Assemblages C and D) formed at conditions similar to those that produced the hornblende-free Assemblage E (Fig. 7). Apart from the grain-boundary replacement of hornblende by staurolite in Assemblage D, calcic amphibole produced at the metamorphic peak is not altered during subsequent retrograde metamorphism.

Retrograde hornblende, however, occurs in KDH5-105 as rims on cordierite and orthoamphibole, together with staurolite, sillimanite, chlorite, and orthoamphibole of different composition to that of the substrate. General reactions describing the retrograde textures are



and



Both reactions occur necessarily below the orthoamphibole solvus (i.e., below 600 °C at pressures of 4–6 kbar; Spear, 1980).

Stability of hornblende with staurolite and sillimanite

Staurolite + hornblende + sillimanite occurs both as a prograde and retrograde assemblage at Copperton. It occurs in rocks of aluminous bulk composition and hence is not related chemographically to the occurrence of kyanite + staurolite + hornblende recorded both by Selverstone et al. (1984) and Helms et al. (1987) in rocks of demonstrably amphibolitic composition. As a prograde phase it is restricted to the edge of domains containing Assemblages D (sillimanite- and staurolite-dominated) and F (cordierite-dominated). The presence of plagioclase in Assemblage D suggests that hornblende is not simply an extra phase stabilized by Ca and Na but is part of an unusual bulk composition resulting from premetamorphic mixing of semipelitic and K-poor peraluminous domains in VA12-A.

The replacement of hornblende by secondary fine-grained staurolite in Assemblage D is problematical, since hornblende + staurolite is already stable. Examination of the boundaries of hornblende grains in VA12-A reveals

minor alteration of hornblende to an assemblage including chlorite, biotite, and quartz (Fig. 2H), whereas the margins of staurolite in the same sample have been altered to chlorite (Fig. 2G). Thus secondary staurolite grew from partly chloritic substrates near hornblende when metamorphic conditions were lower than those required to stabilize staurolite + hornblende + sillimanite, but above those responsible for the stability of chlorite. Secondary staurolite in VA12-A thus belongs to the same metamorphic (reheating) event that produced garnet rims in VA12-B and euhedral garnet upon gedrite + staurolite in G5-B.

The retrograde occurrence in KDH5-105 is fine grained and may not represent an equilibrium assemblage. The assemblage formed in the same domains as sillimanite + gedrite, but, as with the latter, chlorite is normally present, and the division of minerals into those resulting from retrograde hydration and those generated by reheating is not clear.

PRESSURE-TEMPERATURE EVOLUTION

The *P-T* history of orthoamphibole-bearing rocks at Copperton can be interpreted using the petrogenetic grid of Hudson and Harte (1985) for K_2O -poor aluminous pelitic compositions (Fig. 9). The basis for this grid is fully discussed by Hudson and Harte; its use in this paper is more appropriate than the grids of Spear (1978) and Spear and Rumble (1986), since the bulk compositions are closer to those of pelites.

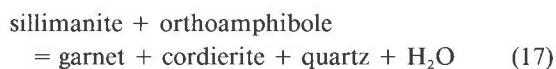
Amphibolite facies retrograde path

In amphibolite facies parageneses (excluding Kielder), the peak conditions lie between the [CHL], (CHL,ALS), and (OAM,CHL) invariant points. In Figure 9, this corresponds to the temperature range 600–625 °C at about 4 kbar, the same range in temperature as calculated for the nearby Annex pelites (Humphreys and Scheepers, 1993). The retrogression can largely be attributed to isobaric cooling through the divariant field staurolite + orthoamphibole + cordierite (by means of Reactions 5 and 6) into the chlorite stability field by Reactions 12 and 3. The shallow slope of Reaction 5 is the most important constraint upon an isobaric path rather than one that simply returns to the origin directly. The formation of kyanite by Reaction 3 suggests that the Hudson and Harte (1985) grid is only partly correctly placed with respect to the aluminum silicate triple point. However, the production of retrograde kyanite in VA12-A, which contains primary sillimanite, is further evidence for isobaric cooling.

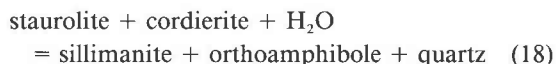
Isobaric cooling at Kielder

Cooling of the granulite facies Assemblage A at Kielder at pressures >5.5 kbar produced the retrograde assemblage sillimanite + orthoamphibole + quartz (Assemblage D*) by Reaction 9 in sample KDH5-105. Isoleths of Reaction 9 are the shallowest of the divariant reactions

discussed here (Fig. 8), and on the Hudson and Harte (1985) grid they would connect the univariant reactions



and



with a near-isobaric slope. Thermobarometric estimates put peak conditions at pressures higher than those defined by Reaction 17, whereas the absence of garnet in KDH5-105 in either prograde or retrograde assemblages indicates that cooling was isobaric to near (above?) the invariant point at which garnet is absent, where chlorite and staurolite resulted from further breakdown of orthoamphibole and cordierite.

Reheating path

The reheating path indicated by the renewed growth of garnet in all three localities must necessarily leave the chlorite stability field. The path indicated on Figure 9 is constrained by the observation that secondary cordierite + orthoamphibole is not produced anywhere from staurolite + chlorite (Reaction 12).

Kinetic factors

The difference in grain size between large prograde grains and commonly small retrograde euhedra supports the dominance of nucleation over grain growth during cooling. This is indicative of the undercooling of peak assemblages into lower *T* stability fields prior to the rapid influx of H_2O . Some stable equilibria may thus have been crossed without leaving any trace of the reaction in the rock record. It is therefore to be expected that the sequence of reactions predicted from the petrogenetic grid does not in every case match the sequence determined from the textures.

TECTONIC IMPLICATIONS

The metamorphic sequence described in Table 2 mirrors the metamorphic evolution of pelites from the nearby Annex deposit (Humphreys and Scheepers, 1993). However, retrogression of high-grade cordierite-bearing assemblages to various combinations of garnet, staurolite, biotite, chlorite, kyanite, and sillimanite is seen up to 300 km along strike to the northwest (Humphreys, 1991) within the Kakamas Terrane (Fig. 1, inset). The typical postpeak pattern throughout the Kakamas Terrane is (1) a period of isobaric cooling from peak pressures of 4–6 kbar followed by (2) rehydration within the kyanite or the lower temperature part of the sillimanite stability fields, and (3) regrowth of garnet, staurolite, and sillimanite from either hydrated (biotite ± chlorite ± kyanite or sillimanite) or unaltered (cordierite, orthopyroxene) substrates. On the bounding thrusts of the Kakamas Terrane, there is clear field evidence linking

REFERENCES CITED

- Baker, J., Powell, R., Sandiford, M., and Muhling, J. (1987) Corona textures between kyanite, garnet, and gedrite in gneisses from Erabiddy, Western Australia. *Journal of Metamorphic Geology*, 5, 357–370.
- Barton, E.S., and Burger, A.J. (1983) Reconnaissance isotopic investigations in the Namaqua Mobile Belt and its implications for crustal evolution: Upington geotraverse. In B.J.V. Botha, Ed., Namaqualand metamorphic complex, p. 173–191. Special Publication of the Geological Society of South Africa, Johannesburg.
- Bence, A.E., and Albee, A.L. (1968) Empirical correction factors for the electron microanalysis of silicates and oxides. *Journal of Geology*, 78, 382–403.
- Cornell, D.H., Hawkesworth, C.J., Van Calsteren, P., and Scott, W.D. (1986) Sm-Nd study of Precambrian crustal development of the Prieska-Copperton region, Cape Province. *Transactions of the Geological Society of South Africa*, 89, 17–28.
- Cornell, D.H., Theart, H.F.J., and Humphreys, H.C. (1990a) Dating a collision-related metamorphic cycle at Prieska Copper Mines, South Africa. In P. Spry and T. Bryndzia, Eds., *Regional metamorphism of ore deposits and genetic implications*, p. 97–116. Coronet, Amsterdam.
- Cornell, D.H., Kroner, A., Humphreys, H.C., and Griffin, G. (1990b) Age of origin of the polymetamorphosed Copperton Formation, Namaqua-Natal Province, determined by single-grain zircon Pb-Pb dating. *South African Journal of Geology*, 93, 709–716.
- Cornell, D.H., Humphreys, H.C., Theart, H.F.J., and Scheepers, D.J. (1992) A collision-related pressure-temperature-time path for Prieska Copper Mines, Namaqua-Natal Tectonic Province, South Africa. *Precambrian Research*, 59, 43–71.
- Dasgupta, S., Sengupta, P., Guha, D., and Fukuoka, M. (1991) A refined garnet-biotite geothermometer and its application in amphibolites and granulites. *Contributions to Mineralogy and Petrology*, 109, 130–137.
- Geringer, G.J., Botha, B.J.V., Pretorius, J.J., and Ludick, D.J. (1986) Calc-alkaline volcanism along the eastern margin of the Namaqua Mobile Belt, South Africa: A possible Middle Proterozoic volcanic arc. *Precambrian Research*, 33, 139–170.
- Gorton, R.K. (1982) Metamorphism of the wall rocks of the Kielder massive sulphide deposit, district of Prieska, N. Cape. *Transactions of the Geological Society of South Africa*, 85, 61–69.
- Harley, S.L. (1984) An experimental study of the partitioning of Fe and Mg between garnet and orthopyroxene. *Contributions to Mineralogy and Petrology*, 86, 359–373.
- (1985) Paragenetic and mineral-chemical relationships in orthoamphibole-bearing gneisses from Enderby Land, eastern Antarctica. *Journal of Metamorphic Geology*, 3, 179–200.
- Helms, T.S., McSweeney, H.Y., Labotka, T.C., and Jarosewich, E. (1987) Petrology of a Georgia Blue Ridge amphibolite with hornblende + gedrite + kyanite + staurolite. *American Mineralogist*, 72, 1086–1096.
- Holdaway, M.J. (1971) Stability of andalusite and the aluminium silicate phase diagram. *American Journal of Science*, 271, 97–131.
- Holland, T.J.B., and Powell, R. (1990) An enlarged and updated internally consistent thermodynamic dataset with uncertainties and correlations: The system K_2O - Na_2O - CaO - MgO - MnO - FeO - Fe_2O_3 - Al_2O_3 - TiO_2 - SiO_2 - C - H_2O . *Journal of Metamorphic Geology*, 8, 89–124.
- Hudson, N.F.C., and Harte, B. (1985) K_2O -poor aluminous assemblages from the Buchan Dalradian, and the variety of orthoamphibole assemblages in aluminous bulk compositions in the amphibolite facies. *American Journal of Science*, 285, 224–266.
- Humphreys, H.C. (1991) The tectonothermal evolution of the eastern Namaqua Province deduced from the petrology and reaction history of metapelites, 420 p. Ph.D. thesis, University of Cape Town, Cape Town, South Africa.
- Humphreys, H.C., and Scheepers, D.J. (1993) Polymetamorphism and isobaric cooling of pelitic schists from the Annex Sulphide Deposit, South Africa. *Journal of Metamorphic Geology*, 11, in press.
- Humphreys, H.C., Scheepers, D.J., and Cornell, D.H. (1988a) Metamorphic studies of kyanite-staurolite schists from Prieska Copper Mines. Geological Society of South Africa 22nd Congress, Durban, Abstracts volume, 299–302.
- Humphreys, H.C., Van Schalkwyk, L., and Scott, W.D. (1988b) A geological and structural map of the Areachap Group succession at Prieska Copper Mines. *South African Journal of Geology*, 91, 373–380.
- Kretz, R. (1983) Symbols for rock-forming minerals. *American Mineralogist*, 68, 277–279.
- Powell, R., and Holland, T.J.B. (1988) An internally consistent thermodynamic dataset with uncertainties and correlations. III. Applications to geobarometry, worked examples and a computer program. *Journal of Metamorphic Geology*, 6, 173–204.
- Robinson, P., Spear, F.S., Schumacher, J.C., Laird, J., Klein, C., Evans, B.W., and Doolan, B.L. (1982) Phase relations of amphiboles: Natural occurrence and theory. In *Mineralogical Society of America Reviews in Mineralogy*, 9B, 1–211.
- Schumacher, J.C. (1991) Empirical ferric iron corrections: Necessity, assumptions and effects on selected geothermobarometers. *Mineralogical Magazine*, 55, 3–18.
- Schumacher, J.C., and Robinson, P. (1987) Mineral chemistry and metasomatic growth of aluminous enclaves in gedrite-cordierite gneiss from southwestern New Hampshire, USA. *Journal of Petrology*, 28, 1033–1073.
- Selverstone, J., Spear, F.S., Franz, G., and Morteani, G. (1984) High pressure metamorphism in the south west Tauern window, Austria: *P-T* paths from hornblende-kyanite-staurolite schists. *Journal of Petrology*, 25, 501–533.
- Spear, F.S. (1977) Phase equilibria of amphibolites from the Post Pond Volcanics, Vermont. *Carnegie Institution of Washington Year Book*, 76, 613–619.
- (1978) Petrogenetic grid for amphibolites from the Post Pond and Ammonoosuc Volcanics. *Carnegie Institution of Washington Year Book*, 77, 805–808.
- (1980) The gedrite-anthophyllite solvus and the compositional limits of orthoamphibole from the Post Pond Volcanics, Vermont. *American Mineralogist*, 65, 1103–1118.
- Spear, F.S., and Rumble, D., III (1986) Pressure, temperature and structural evolution of the Orfordville Belt, west-central New Hampshire. *Journal of Petrology*, 27, 1071–1093.
- Theart, H.F.J. (1985) Copperton Areachap Cu-Zn mineralization, 200 p. Ph.D. thesis, University of Stellenbosch, Stellenbosch, South Africa.
- Visser, D., and Senior, A. (1990) Aluminous reaction textures in orthoamphibole-bearing rocks: The pressure-temperature evolution of the high-grade Proterozoic of the Bamble Sector, south Norway. *Journal of Metamorphic Geology*, 8, 231–246.
- Williams, M.L., and Grambling, J.A. (1990) Manganese, ferric iron and the equilibrium between garnet and biotite. *American Mineralogist*, 75, 886–908.

MANUSCRIPT RECEIVED JANUARY 13, 1992

MANUSCRIPT ACCEPTED APRIL 30, 1993